

A polycaprolactone-based syntactic foam with bidirectional reversible actuation

Lu Lu,¹ Jinbao Cao,² Guoqiang Li¹

¹Department of Mechanical & Industrial Engineering, Louisiana State University, Baton Rouge, Louisiana 70803

²Department of Chemistry, Louisiana State University, Baton Rouge, Louisiana 70803

Correspondence to: G. Li (E-mail: lguoq1@lsu.edu)

ABSTRACT: A polycaprolactone (PCL) based syntactic foam was prepared by incorporating 40% by volume of glass microspheres and crosslinking the PCL matrix with benzyl peroxide. FTIR, differential scanning calorimeter, scanning electron microscopy, dynamic mechanical analysis, and material testing system were employed to elucidate the chemical, thermal, surface, and mechanical properties of the syntactic foam. This crosslinked PCL (cPCL) syntactic foam displayed a clear two-way shape memory effect (2W-SME). Specifically, around 10% elongation upon cooling and 10% contraction upon heating were observed for the system at selected external loads and temperature windows. Programming was shown to be the key parameter to tune a prominent 2W-SME of the cPCL syntactic foam. With the combined physical/mechanical properties (low density, ductile, high compressive strength, water tightness, etc.), together with its bidirectional reversible actuation, the system developed may be good for broad applications in different fields such as biomedical devices, soft robots, aircrafts, and sealants. © 2017 Wiley Periodicals, Inc. *J. Appl. Polym. Sci.* **2017**, *134*, 45225.

KEYWORDS: bidirectional reversible actuation; polycaprolactone; two-way shape memory

Received 20 January 2017; accepted 18 April 2017

DOI: 10.1002/app.45225

INTRODUCTION

Due to the high demands for lightweight, insulating, ductile, soft, shock, and sound absorbing materials, investigation of polymeric foams has been an attractive research topic since 1931, when the first polymer foam was developed.¹ Polymer foams are commonly seen in our daily life with a variety of applications such as packaging or cushioning for fragile items and insulation materials. Polymeric foams consist of polymer matrix with either air bubbles or air tunnels. To generate the air bubbles or tunnels, low boiling point organic liquid, or chemical foaming agent such as thermally unstable substances were used as blowing agents when polymeric foams were prepared.^{2,3} Some foaming agents (i.e., organic liquid) can cause environmental concerns considering the large-scale production of polymer foams every year. An effective and popular alternative was developed to use nitrogen or carbon dioxide as blowing agents.^{2,4,5}

Polyurethane,^{6,7} polystyrene,^{5,8} epoxy,^{9–11} starch^{12,13} etc. have been foamed for target applications. Polymer nanocomposite foams, which contain nanoparticles/clays, attracted increasing attention as a result of the enhanced mechanical performance along with other merits.^{14–16} Due to the promising potential applications of polycaprolactone (PCL) in drug delivery and medical materials for artificial skin or bone,^{17,18} PCL foams

have been investigated and prepared via different foaming agents. Supercritical carbon dioxide,^{17,19} mixtures of carbon dioxide and nitrogen gases,^{20,21} or combination of gas foaming and microparticulate templating²² are examples of screened foaming agents. In addition, PCL/nanoparticle and PCL/clay nanocomposites have also been prepared through supercritical carbon dioxide foaming.^{23,24} The aforementioned gas foaming strategies for the preparation of PCL foam were widely adopted, attributing to its reduced side effects to biological systems for *in vivo* applications as compared to organic liquid-based method.

Another merit of PCL is its shape memory effect. It can restore its permanent shape from deformed state by external stimuli (i.e., temperature). Traditional shape memory polymer (SMP) can only “memorize” one temporary shape in every shape memory cycle. However, two-way SMP is capable of undergoing reversible actuation, i.e., elongation upon cooling and contraction upon heating, with only one-time programming or even without a particular programming but with a constant tensile load.²⁵ Two-way shape memory effect (2W-SME) was firstly discovered in liquid crystalline elastomers.²⁶ Other polymeric systems such as polyethylene,^{27,28} polyurethane,^{29–34} polyester,³⁵ epoxy,^{36,37} ionomer Nafion,³⁸ polycyclooctene,^{39–41} poly(ethylene-co-vinyl acetate),^{42,43} etc.^{44–49} have also been demonstrated to display 2W-SMEs. Among these polymers, PCL was widely

studied for its 2W-SMEs due to its potential bio-applications.^{50–59} Mather and coworkers prepared a highly porous foam scaffolds through crosslinking PCL and poly(ethylene glycol) and modified porogenleaching technique.⁵⁹ This foam exhibited reversible actuation under compression. However, the mechanical strength of the foam was not discussed in this work.

The 2W-SME, i.e., reversible bidirectional shape memory effect, enabled applications such as self-sufficient grippers, fixator, fastening devices, cell encapsulation, swimmers, optical gratings, soft actuators, morphing structures, self-healing materials, sealant, etc.^{34,46,56,60}

One limitation with open-celled polymeric foam persists in its low strength and water absorption, which may restrict its applications to high moisture environments such as underwater structures, outdoor structures such as sealant for expansion joint in concrete pavement or bridge deck,^{61,62} etc. Hollow microspheres filled polymer composites, also known as syntactic foams, have been intensively studied over the past five decades due to their high strength, dimensional stability, and low moisture absorption compared to open-celled foams.^{10,63–69} The hollow microspheres include glass microspheres (microballoon), polymeric microspheres, metallic microspheres, and ceramic microspheres.⁶⁰

However, there is currently a lack of understanding of two-way SMP based syntactic foam in general and PCL-based syntactic foams in particular, including physical, mechanical, and reversible actuation properties. Herein, the first example of PCL-based syntactic foam with 2W-SME under tensile load will be discussed in this work. Glass microspheres were employed to foam the PCL. The physical, mechanical, morphological, and reversible actuation behavior will be investigated.

EXPERIMENTAL

Materials

The PCL used in the experiment was Capa™ 6506 from Perstorp (Industriparken, Sweden). It is a high-molecular-weight linear polyester supplied in powder form. The molecular weight is 50,000 g/mol and the density is 1.1 g/cm³. Q-CEL 6014 hollow glass microspheres was purchased from Potters Industries LLC (Barnsley, United Kingdom). The effective density is 0.14 g/cm³ and the mean particle size is 85 μm with size ranging from 5 to 200 μm. The maximum working pressure for the glass spheres is 1.72 MPa. Benzoyl peroxide (BPO) and tetrahydrofuran (THF) were ordered from Sigma-Aldrich (St. Louis, MO) and used without further purifications.

Synthesis of the Two-Way Shape Memory Syntactic Foam

PCL powder of 80 g and THF of 90 mL were firstly mixed well in a 250-mL beaker. Glass spheres of 4.1 g (40% by volume of PCL) and BPO of 8 g (crosslinking agent) were then added into the beaker. The mixture was thoroughly but slowly blended for at least 10 min to avoid generating large air bubbles. The mixture was then poured into a polytetrafluoroethylene (PTFE) mold and placed in a hood to allow air dry for 1 day. The mold was then capped and clamped at four corners to cure the mixture at 140 °C for 20 min. The procedure was modified from previous literature due to the incorporation of glass

microballoons.⁵⁰ The cured mixture was then allowed to cool down slowly overnight. A piece of white solid foam, i.e., crosslinked PCL (cPCL) syntactic foam was produced. The density of the foam is ~0.7 g/cm³, determined from the mass and the volume measurements. The mass was measured by a high accuracy balance (10⁻⁵ g, XS105, Mettler Toledo, Italy), while the volume was determined by displacement method. Similarly, crosslinked PCL without glass microspheres was also prepared under the same condition as control. The density of the cPCL is ~1.1 g/cm³.

Chemical and Thermal Analysis

The chemical composition of the as-prepared cPCL foam was characterized with FTIR using Nicolet 6700 spectrometer with the scan range of 4000–600 cm⁻¹ (Thermo Scientific, Waltham, MA). Differential scanning calorimeter (DSC) studies were conducted using TA DSC 2920 (TA Instruments, DE). Samples of about 5–10 mg were each placed in an aluminum pan and scanned between -58 °C and 90 °C. The second heating curve and first cooling curve are shown in the plot. The heating and cooling rates of the DSC were 10 °C/min. The purging rate of the nitrogen gas was 30 mL/min.

Surface Visualization at Microscale

The as-prepared cPCL foam and cPCL were visualized with scanning electron microscopy (SEM) (Quanta 3D FEG, Hillsboro, OR) using secondary electrons. The sample surfaces were coated with platinum for about 6 nm. The accelerating voltage was 5 kV and the working distance was 9–9.5 mm.

Temperature Scan and Shape Memory Studies

Dynamic mechanical analysis (DMA) Q800 (TA Instruments, DE) was used to run the temperature sweeps for the cPCL foam and cPCL. It was also used to investigate the one-way and two-way shape memory effect of the cPCL foam. The temperature sweeps were conducted in the multi-frequency-strain mode using the tension clamp of Q800. The amplitude was 15 μm, the frequency was 1 Hz, and the temperature sweep range was -60 to 60 °C. The temperature ramp rate was 3 °C/min. The two-way shape memory studies were conducted by tuning temperature windows, external load, and programming levels during the heating and the cooling cycles to study their influence on the actuation levels. One-way shape memory studies were also conducted with three heating and cooling cycles to calculate the shape fixity (F) and the shape recovery ratios (R). The shape fixity (F) and the shape recovery (R) ratios were calculated using eqs. (1) and (2), respectively.

$$F = 100\% \times \varepsilon_f / \varepsilon_s \quad (1)$$

$$R = 100\% \times (\varepsilon_f - \varepsilon_r) / \varepsilon_f \quad (2)$$

where ε_s is the prestrain under load, ε_f is the fixed strain after cooling and load removal, and ε_r is the recovered strain.

The coefficient of thermal expansion (CTE) of the cPCL foam and the cPCL was also studied with DMA. The materials were subjected to heating and cooling without external load to monitor their natural responses to thermal change. For DMA studies, all materials were cut into thin films with a dimension around 10 mm × 7 mm × 2 mm (length × width × thickness).

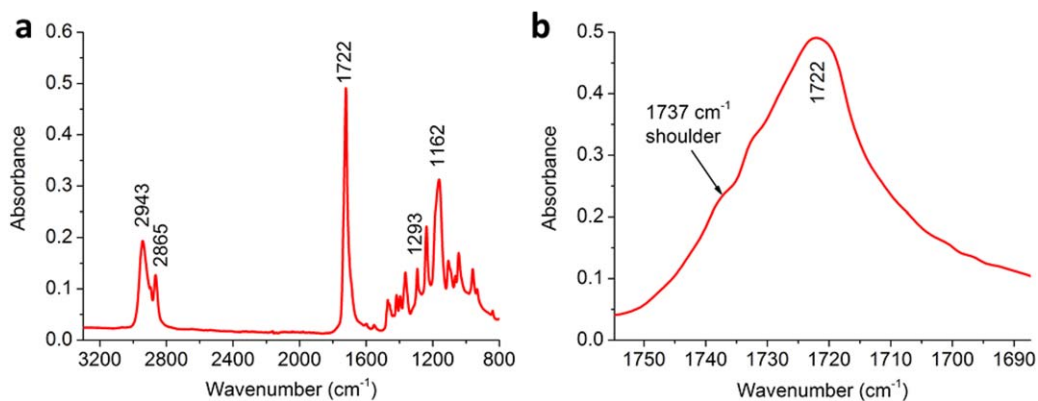


Figure 1. Full (a) and zoom-in (b) views of the FTIR spectra of cPCL foam. [Color figure can be viewed at wileyonlinelibrary.com]

Compression Test

Hot compression tests for cPCL foam and cPCL at 50 °C were performed using eXpert 2610 MTS (ADMET, Norwood, MA). The control software is MTESTQuattro. The temperature in the thermal chamber was controlled by E5AC-T digital controller (OMRON, Japan). The crosshead test speed was 1 mm/min. The data acquisition rate was 1 Hz. The temperature of the thermal chamber was first stabilized at 50 °C. The cPCL foam and the cPCL were then compressed to 76% strain, respectively (i.e., after compression the height was 24% of its original height). The stress during the process was closely monitored.

Stress Recovery Test

To investigate the recovery forces of the cPCL foam and the cPCL, the materials were firstly cut into samples with dimensions around 10 mm × 20 mm × 13 mm and then compressed to 80% strain at room temperature using the MTS machine (Alliance RT/5, MTS, USA). The instrument preload was 2.2 N and the crosshead test speed was 1 mm/min. The data acquisition frequency was 10 Hz. The samples were held at the 80% strain position for 13 min for structural and stress relaxation, followed by temperature rising to 50 °C to induce the stress recovery of the samples. During the test, the samples were still constrained in between the MTS crosshead without allowing shape recovery, leading to fully constrained stress recovery. As the test proceeded, the recovery force was tracked and recorded by the MTS machine. The data acquisition frequency was 3 Hz for stress recovery test.

X-ray Diffraction

The X-ray diffraction (XRD) analysis was performed on a Panalytical Empyrean diffractometer by using Cu as the anode material. The samples were scanned from 5° to 55° in a step size of 0.026° with generator voltage of 45 kV and current of 40 mA at room temperature.

RESULTS AND DISCUSSION

Chemical Analysis of the Synthesized cPCL Foam with FTIR

The full and zoom-in FTIR spectra of the cPCL foam are shown in Figure 1. The characteristic peaks of PCL are identified in Figure 1(a) at 2943 cm⁻¹, 2865 cm⁻¹, and 1722 cm⁻¹, which correspond to asymmetric CH₂ stretching, symmetric CH₂ stretching, and carbonyl stretching, respectively. The

semicrystalline nature of the cPCL is verified by the multimodal nature of the carbonyl peak as viewed in Figure 1(b). The sharp stretching peak at 1722 cm⁻¹ is associated with carbonyl stretching in the crystalline domain.⁷⁰ The shoulder at 1737 cm⁻¹ results from carbonyl stretching in the amorphous domain.⁷⁰ This is further verified by signals in the fingerprint region. For instance, the 1293 cm⁻¹ peak is associated with C—O and C—C stretching in the crystalline domain, while 1162 cm⁻¹ can be assigned to C—O and C—C stretching in the amorphous region.^{70,71}

Thermal Analysis

DSC thermograms of the second heating cycle and the first cooling cycle of the four specimens are shown in Figure 2. The first heating cycles are not displayed because the thermal history of the raw materials is always shown on the first heating cycles. The four samples are cPCL foam, 280% tensile programmed cPCL foam (280% was selected to have a sufficiently tensile programmed sample in the group to evaluate the effect of programming levels), cPCL, and PCL powder reagent. The glass transition of the purchased PCL powder reagent used in the experiment is around -60 °C, which is provided by the manufacture. It is close to the detection limit of the DSC instrument as the cooling cycle can only go down to -58 °C.

The cPCL foam has the lowest melting point (47.0 °C) within these four specimens, followed by 280% programmed cPCL foam (49.8 °C), cPCL (51.6 °C), and PCL powder reagent (56.3 °C) as given in Table I. The melting temperature for semicrystalline polymer PCL after partial crosslinking is decreased. This is because crosslink reduces the chain length and mobility between the two neighboring crosslink points, preventing large and perfect crystals from forming, and leading to lowered melting temperature. Therefore, the PCL reagent prior to crosslinking has the highest melting point. Crosslinked PCL foams [Figure 2(a,b)] have lower melting points than cPCL [Figure 2(c)] itself. This is due to decrease in crystallinity after adding 40% by volume glass spheres. Tensile programmed cPCL foam has higher melting point than the non-programmed foam. The difference is because tensile programming induced better chain alignment and consequently higher crystallinity (strain induced crystallization) and melting point of the material.²⁵ The trend for the comparison of the crystallization temperatures among

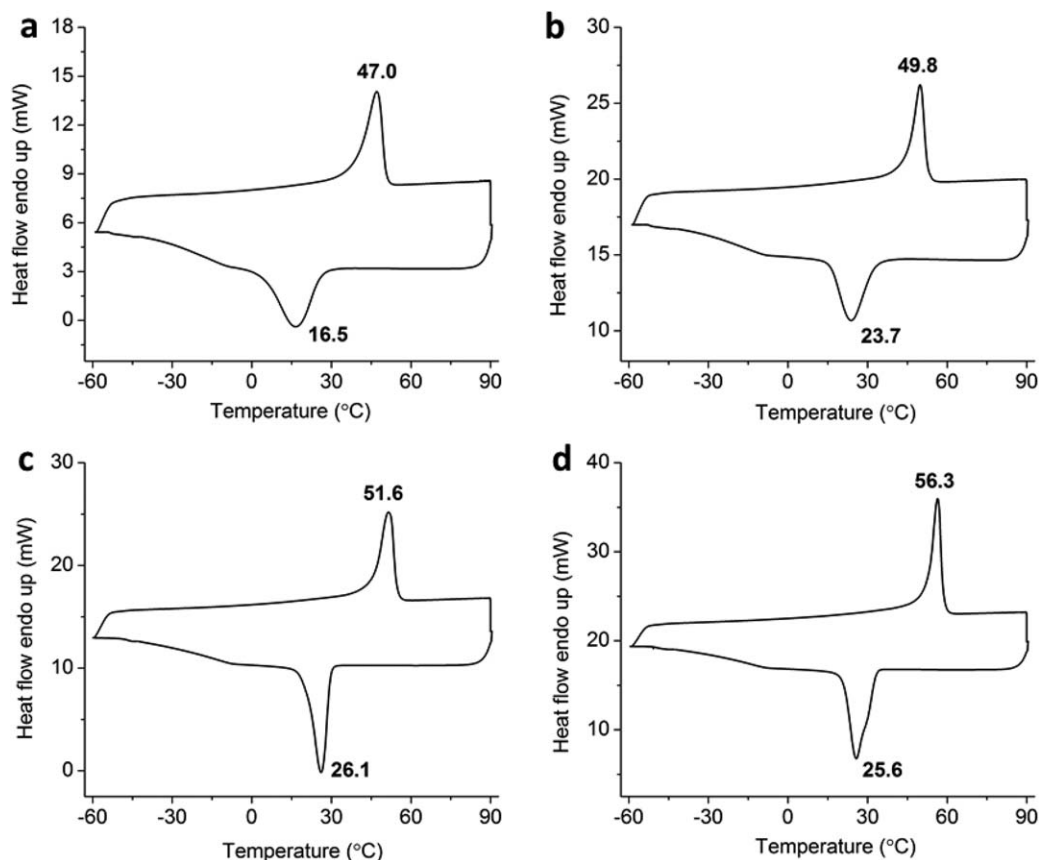


Figure 2. DSC thermograms of (a) cPCL foam, (b) tension programmed cPCL foam, (c) cPCL, and (d) purchased PCL reagent. The second heating and the first cooling cycles are shown in the plots.

the four samples is similar to that of the melting temperatures. The enthalpy is proportional to the crystallinity of the samples, which means that the programmed cPCL foam has the highest crystallinity, followed by the PCL reagent, the cPCL, and the cPCL foam.

Surface Visualization of cPCL Foam and cPCL with SEM

As structure relates closely to materials properties, it is important to elucidate the microstructures of the newly synthesized foams. High resolution SEM was employed to visualize the cPCL foam and cPCL. For the cPCL foam sample, both glass spheres and surrounding polymer matrix can be visualized by SEM [Figure 3(a,b)]. In Figure 3(a), the glass sphere is almost hiding in the matrix, and in Figure 3(b) it is on the matrix surface. For the cPCL sample, a much smoother surface with the line features can be seen [Figure 3(c,d)].

Comparison of the Thermomechanical Property of cPCL Foam and cPCL

A big difference was observed when scanning the cPCL foam and the cPCL films from -60 to 60 °C with DMA as shown in Figure 4. The glass transition temperatures of the materials are acquired on the basis of the onset of storage modulus, the peak of loss modulus, and the peak of tan delta. There is usually a difference among the three T_g values. The T_g values for the cPCL foam are higher than that for the cPCL, which is due to the 40% volume fraction of the glass spheres. The glass spheres

have a reinforcing effect and the mobility of the PCL chains in the interphase region between the polymer matrix and the glass spheres are affected and lowered.⁷² For both storage modulus and loss modulus, the reduction in modulus values with increasing temperature is much lower for the cPCL syntactic foams, suggesting better thermal stability.

Two-Way Shape Memory Effect of the cPCL Syntactic Foam

PCL is known to display 2W-SME.^{50–59} It is interesting to know the 2W-SME of the cPCL syntactic foam because of the better thermal stability and lower cost of the composite. The two-way shape memory performance of the cPCL syntactic foam was studied using DMA by tuning temperature ranges, external loads, and tension programming levels. Programming is a process to obtain the chain segment orientation and the

Table I. Comparison of the Thermal Properties of the Four Samples from Figure 2

	Melting point (°C)	Crystallization point (°C)	Enthalpy (J/g)
cPCL foam	47.0	16.5	14.2
Programmed cPCL foam	49.8	23.7	84.8
cPCL	51.6	26.1	31.5
PCL reagent	56.3	25.6	54.5

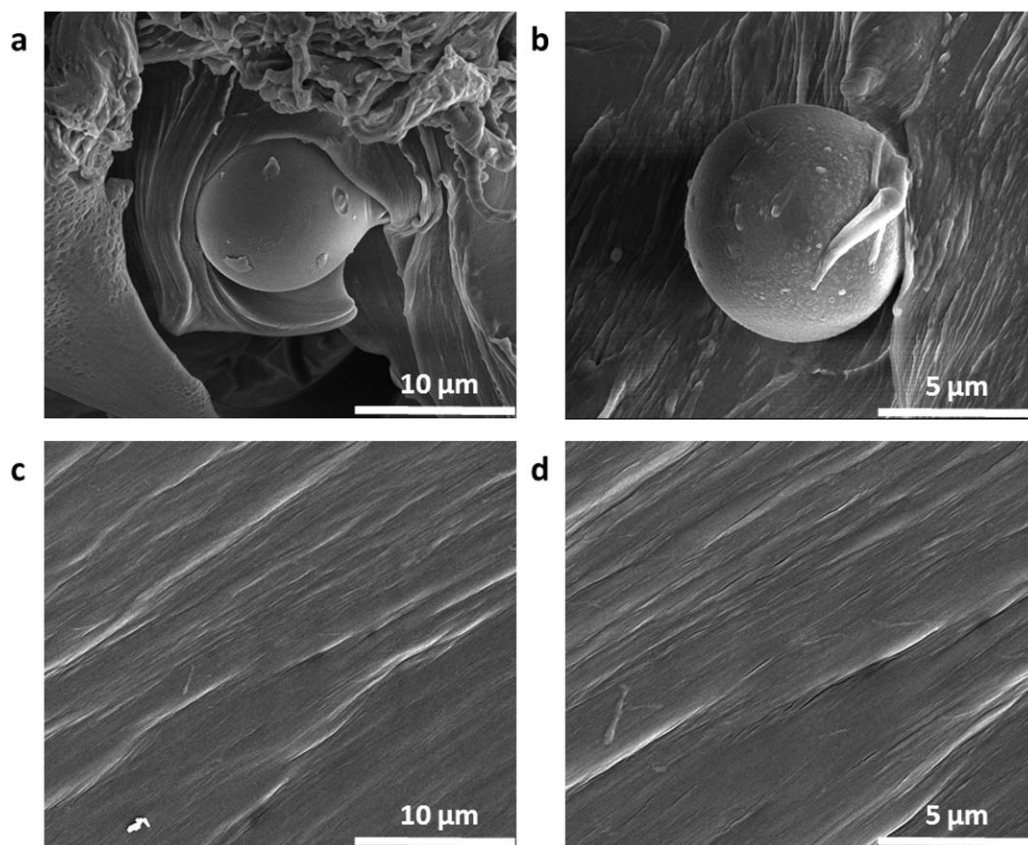


Figure 3. SEM photographs of cPCL foam containing glass spheres (a and b) and the relative smooth cPCL surface (c and d).

macroscopic shape shifting geometry.⁷³ It is noted that the programming load is different from the constant load used to induce 2W-SME. When conducting programming, the material is either stretched or compressed at an elevated temperature above the glass transition temperature (hot programming) or below glass temperature (cold programming). Then the temperature is slowly cooled down with the load. Finally, the programming load will be removed at the end of the programming process. However, constant load is the external force maintained on the material during the entire thermomechanical cycles.

An example of the two-way shape memory study is displayed in Figure 5. The full plot is shown in Figure 5(a). For easier visualization of the plot details, the zoom-in views of the first half of the tuning process is displayed in Figure 5(b) and the second half of the stabilized 2W-SME process is shown in Figure 5(c). First, a thin film of the cPCL foam was programmed (elongated) to 134% at 55 °C with 0.043 MPa load. The material was then cooled down to 25 °C at a cooling rate of 10 °C/min to fix the programmed shape. Afterwards, the 2W-SME working temperature range and external load were tuned to investigate their influences on the 2W-SME performance of the syntactic foam.

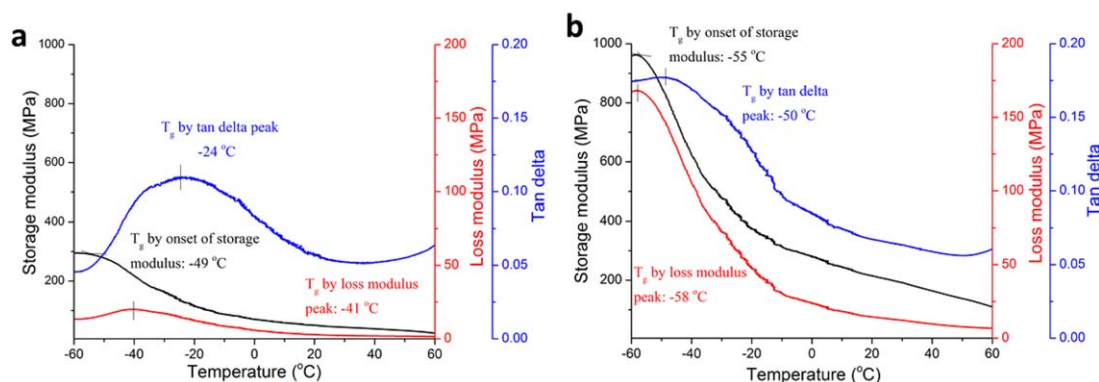


Figure 4. Temperature sweeps of (a) cPCL foam and (b) cPCL acquired with DMA. The Y-axis is set the same for comparison. [Color figure can be viewed at wileyonlinelibrary.com]

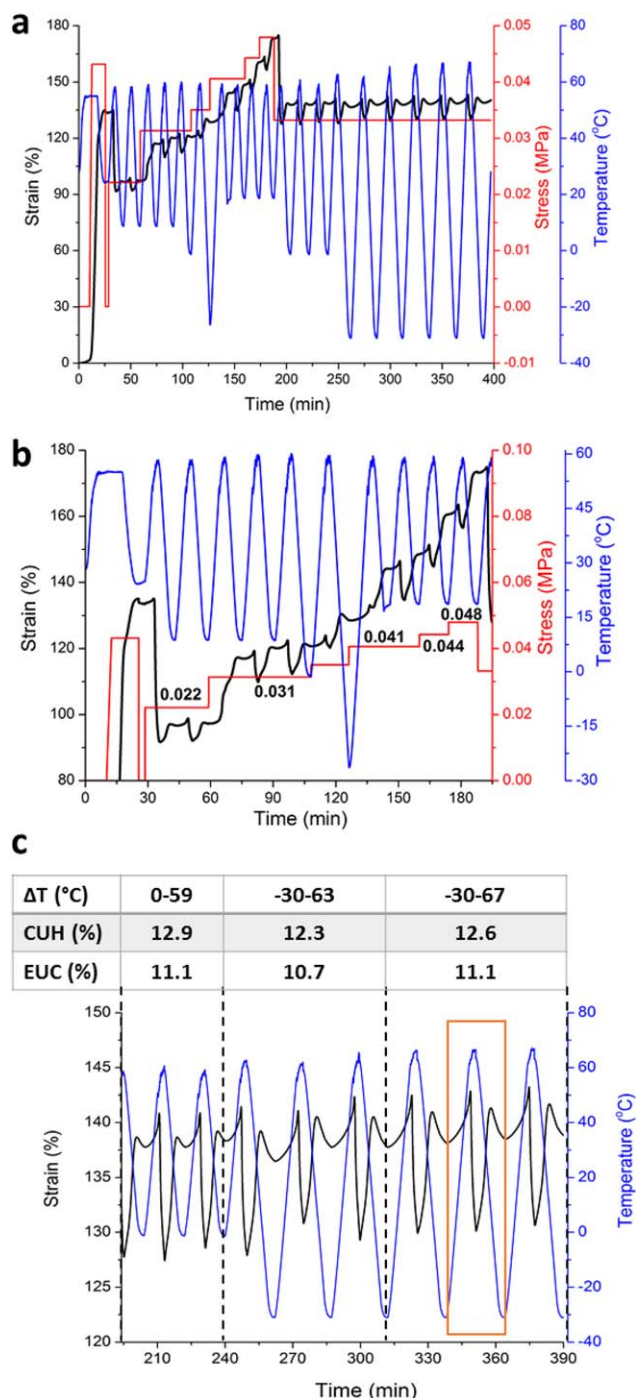


Figure 5. Two-way shape memory effect of the cPCL syntactic foam. (a) Full plot. (b) The first half of the plot. (c) The second half of the plot. The temperature range (ΔT), contraction upon heating (CUH), and elongation upon cooling (EUC) values are listed above the figure c. [Color figure can be viewed at wileyonlinelibrary.com]

In the zoom-in view [Figure 5(b)], when increasing the load from 0.022 to 0.031 MPa while keeping the temperature range the same, the expansion upon cooling increased from 5.3% to 10.4% and the contraction upon heating increased from 4.7% to 10.2%. When increasing the external loads to 0.041, 0.044, and 0.048 MPa, the strain range shifted to higher values as the

cycle number increased. This is a result of excessive external load when inducing the 2W-SME. Therefore, the load was kept at 0.033 MPa while investigating the 2W-SME with the change of temperature ranges [Figure 5(c)]. Three temperature ranges (ΔT) were selected as shown in Figure 5(c). The calculated elongation upon cooling and contraction upon heating are listed in the table above [Figure 5(c)]. It was noticed that expanding the working temperature window of the 2W-SME from 0 to 59°C to -30 to 67°C does not increase the strain actuation. This is because the cPCL has a relatively narrow melting (33.4–51.9°C) and crystallization (2.3–28.9°C) transitions based on the DSC test results. Because the 2W-SME is based on the melting and crystallization transition of the crystalline domains, widening the temperature window out of the transition zone does not contribute to further enhancing the 2W-SME. In other words, it is also possible that the strain reversible actuation of the 2W-SME is only large enough to compensate for the normal physical behavior (contraction upon cooling and expansion upon heating) of glass microspheres in the temperature range from 0 to -30°C or from 59 to 67°C.

Interestingly, a phenomenon was observed within the two-way shape memory cycles of the syntactic foam in the orange box in Figure 5(c). When heating from -30 to 63°C, the syntactic foam elongated by 4.9%. Then the foam contracted by 12.8% when kept heating the material from 63 to 67°C. When cooling the foam from 67 to 8°C, it elongated by 11.2%. Then the material contracted 3.0% when keeping cooling from 8 to -30°C. Therefore, the overall actuation of the 2W-SME is around 8%. The similar phenomenon was observed in a PCL-POSS (POSS: polyhedral oligomeric silsesquioxane) double network,⁵⁷ a copolyester urethane network,³⁴ and a polydopamine-graft-PCL system⁵⁸; however the authors did not discuss about the phenomenon. We think the reason is that the cPCL has a relatively narrow melting (33.4–51.9°C) and crystallization (2.3–28.9°C) transitions. Only when the temperature is within the transition zones, the material displays the 2W-SME; outside the transition zones, it behaves as a regular material, which elongates upon heating and contracts upon cooling.

The CTE of the cPCL foam and the cPCL were studied to investigate the materials behavior in response to temperature change without the influence of the external load. The CTE study results are shown in Figure 6. Both the cPCL foam and the cPCL were subjected to four heating and cooling cycles. In the first heating cycle, both samples displayed clear strain increase. Then the strain tends to stabilize. The last three cycles were used to calculate the CTE of both samples. The cPCL foam elongated to 1.1% when heated from -10 to 65°C. It elongated another 0.4% when cooled from 65 to 45°C. Continuous cooling of the cPCL foam to -30°C led to a contraction by 1.4%. Heating the sample from -30 to -10°C resulted in a further contraction of 0.1%. Therefore, after one heating and cooling cycle, the strain change is 0% which means the material went back to its original length. The CTE value, which is equal to strain over temperature, is $1.5 \times 10^{-4} \text{ C}^{-1}$ ($1.1\% / (65 + 10) \text{ }^\circ\text{C} = 1.5 \times 10^{-4} \text{ C}^{-1}$).

For the cPCL film, heating the material from -10 to 65°C led to an elongation of 1.4%. Then, cooling the cPCL from 65 to

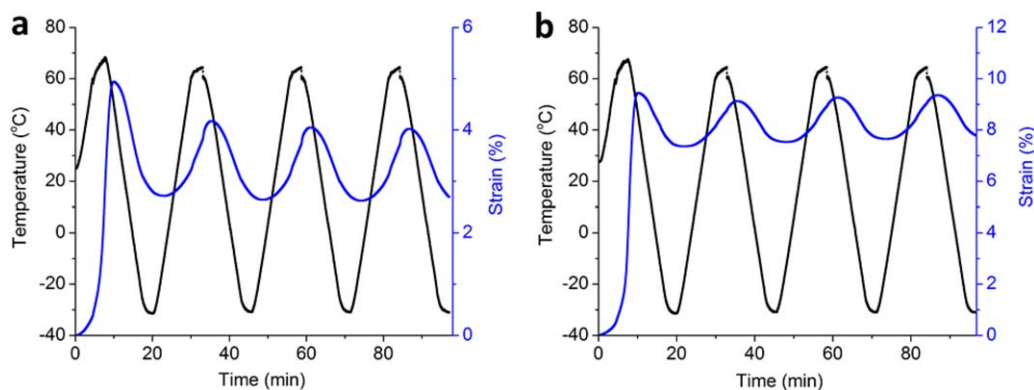


Figure 6. CTE of (a) the cPCL foam and (b) the cPCL. [Color figure can be viewed at wileyonlinelibrary.com]

45 °C led to another elongation by 0.4%. Continuously cooling the material from 45 to -30 °C resulted in a contraction of 1.5%. Then heating the sample from -30 to -10 °C contributed to a 0.1% contraction. Overall, the cPCL film elongated 0.2% after one complete heating and cooling cycle and the CTE value is $1.9 \times 10^{-4} \text{ C}^{-1}$ ($1.4\%/(65 + 10) \text{ }^\circ\text{C} = 1.9 \times 10^{-4} \text{ C}^{-1}$).

After the comparison of the CTE effects between the cPCL foam and the cPCL, it came to the conclusion that: (1) the elongations upon cooling are 0.4% and contractions upon heating are 0.1% for both samples, which indicates that non-programmed/as-prepared cPCL foam and cPCL have small 2W-SMEs; (2) the contraction upon cooling and elongation upon heating for both materials are similar, in the order of 10^{-4} C^{-1} .

The cPCL foam was tensile programmed to 134% strain level and the 2W-SME was observed immediately following the programming step in Figure 5. What would happen when investigating the 2W-SME at a lower tensile programming level? The experiment result is shown in Figure 7. First, the cPCL foam was stretched to 46% strain. Then the external load was increased stepwise from 0.043 to 0.065 and then to 0.077 MPa. However, no clear 2W-SME, i.e., material contraction upon heating and elongation upon cooling, was observed. During the cycle which indicated with a black arrow, an obvious creep effect was observed when the cPCL foam was stretched to 82%. The material demonstrated the 2W-SME with 2.9% contraction upon heating and 17.5% elongation upon cooling, which resulted from a creep effect under excessive external load. When the external load was reduced back to 0.065 MPa, the 2W-SME was observed for the entire time. However, the 2W-SME was only relatively stable for the first three cycles. A creep effect was seen for the rest four cycles. This study indicates that a sufficient tensile programming is necessary for the cPCL foam to display clear 2W-SME without creep.

One-Way Shape Memory Effect

In addition to the 2W-SME, PCL is known to show one-way shape memory effect (1W-SME).⁷⁴ Hence, 1W-SME of the PCL foam was also investigated in this study by tension programming and monitoring its shape recovery at the programming

temperature for three cycles. For the tension programming step, the cPCL foam was first heated to 55 °C, and then a tensile load was applied to stretch the sample to 163%, 205%, and 258% strain for each programming cycle, respectively. The sample was then cooled down to room temperature to fix the temporary shapes. Afterwards, the load was removed and the temperature was elevated to 55 °C to induce shape recovery. The shape fixity ratios and the shape recovery ratios for the three shape memory cycles are listed in Figure 8, from which high shape fixity and shape recovery ratios of the cPCL foam can be seen. Besides, the shape recovery ratio increased to almost 100% after the 1st cycle, this is also commonly seen in SMPs.^{25,75}

Stress Recovery

Recovery force is an important index/parameter when evaluating SMPs. Herein, the recovery force of the cPCL syntactic foam was also studied. As a comparison, both the cPCL foam and the cPCL were compression programmed to 80% strain at room temperature (defined as cold programming, which was below the melting transition temperature), and were held at this strain level for 13 min. The stress of the cPCL foam was 23.2 MPa when compressed to 80% strain, which slowly reduced to 16.8 MPa in 13 min. In contrast, the stress of the cPCL was

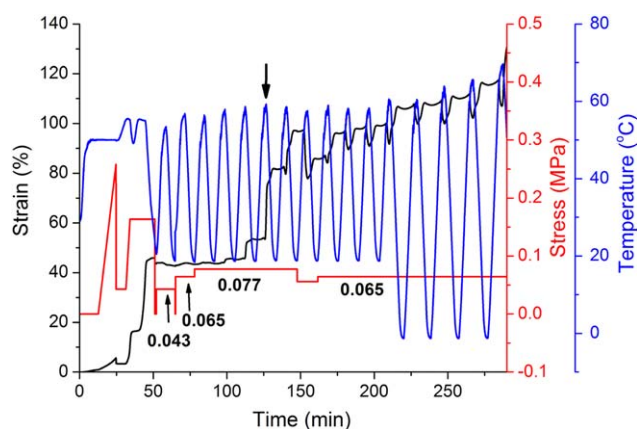


Figure 7. The influence of programming level on the 2W-SME of the cPCL syntactic foam. [Color figure can be viewed at wileyonlinelibrary.com]

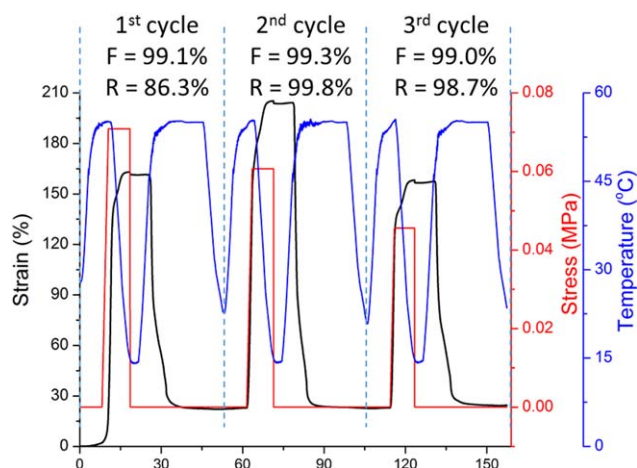


Figure 8. Three shape memory cycles of the cPCL foam. The shape fixity ratios and shape recovery ratios are labeled in each cycle. [Color figure can be viewed at wileyonlinelibrary.com]

87.5 MPa initially, which slowly dropped to 65.3 MPa in 13 min. The stiffness of the cPCL is higher than the cPCL foam at room temperature as indicated by the compression test. This can be attributed to the presence of air bubbles and tunnels in the foam as evidenced by the SEM. This is also consistent with shape memory epoxy based syntactic foam.⁶⁷ During the stress recovery process, the crosshead of the material testing system

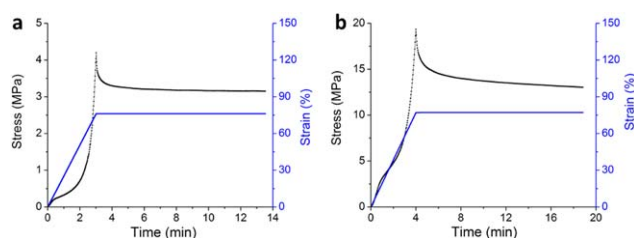


Figure 10. Hot compression of the cPCL foam (a) and the cPCL (b) at 50°C using MTS. [Color figure can be viewed at wileyonlinelibrary.com]

(MTS) was kept in close contact with the compressed material without applying external load. Then the environment temperature was elevated to 50°C to induce shape recovery. The force generated during the materials recovery process was recorded and plotted in Figure 9(b,d). For the cPCL foam, the recovery force reached the maximum value 0.19 MPa in 26 min, followed by a slow drop to 0.18 MPa in 48 min. As a comparison, the recovery force reached the maximum at 0.83 MPa after 74 min for the cPCL. The faster response in the cPCL foam is presumably due to more efficient heat conduction due to the 40% by volume glass microspheres. The lower maximum recovery force for the cPCL foam can be attributed to the enclosed air bubbles within the microballoons.

No crack formation was observed during the compression even up to 90% of the strain for both samples. This serves as a good

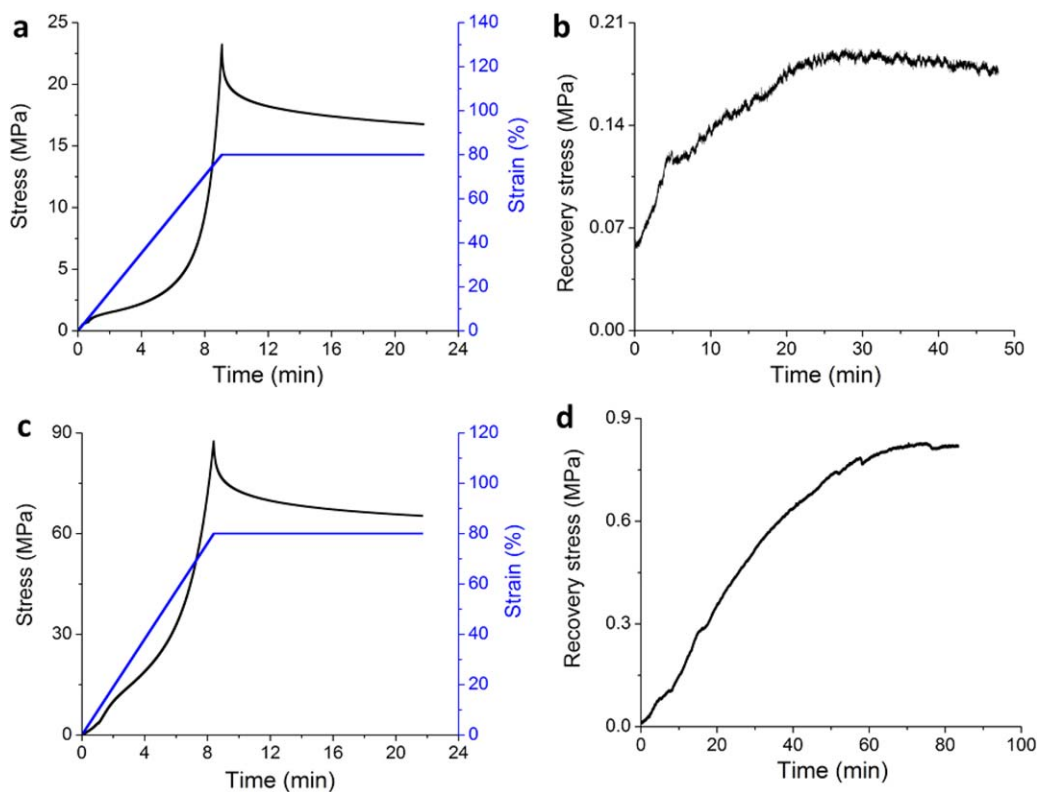


Figure 9. Programming and stress recovery studies of the cPCL foam (a and b) and the cPCL (c and d). (a) Compressive programming of the cPCL foam till 80% strain. (b) Tracking of the recovery stress of the programmed cPCL foam. (c) Compressive programming of the cPCL. (d) Monitoring the recovery stress of the compressed cPCL. [Color figure can be viewed at wileyonlinelibrary.com]

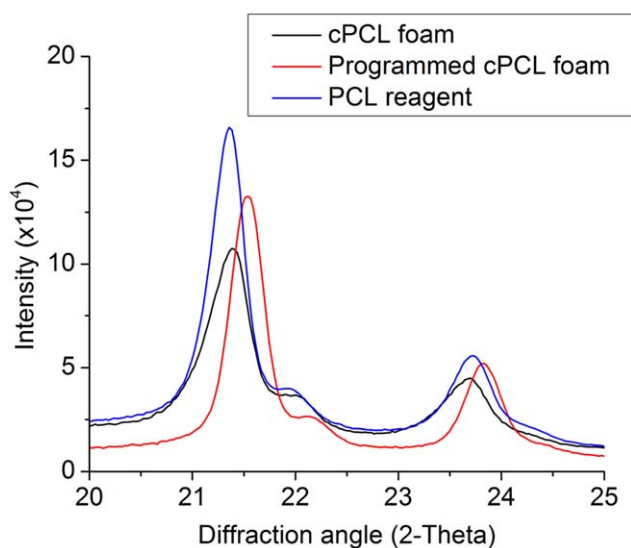


Figure 11. XRD intensity profiles of the cPCL foam, programmed cPCL foam, and PCL reagent. [Color figure can be viewed at wileyonlinelibrary.com]

demonstration of the relatively soft and flexible nature of PCL materials. The shape fixity ratio is 53% for the cold programmed cPCL foam and 57% for the cPCL. The shape recovery ratios are 50% and 60% for the cPCL foam and the cPCL, respectively. The lower shape fixity ratio and shape recovery ratio are common for cold programmed one-way SMP or SMP-based syntactic foam.^{76,77}

The compression experiment was also conducted at 50 °C using as-prepared cPCL foam and cPCL. The results are shown in Figure 10. When compressing the cPCL foam to 76% strain, the stress reached to 4.2 MPa and then stabilized at 3.2 MPa. When compressing cPCL to the same level, the stress was 18.6 MPa and dropped to 13.0 MPa in 14 min. This indicates that the cPCL is also stiffer than the cPCL foam at 50 °C.

Table II. Analysis of XRD Results

Sample	Crystallinity (%)	Full width at half maximum (°)
cPCL foam	44.8	0.47
Programmed cPCL foam	61.3	0.39
PCL reagent	50.9	0.39

XRD Analysis

The XRD analysis was done for the cPCL foam, the programmed cPCL foam and the PCL reagent to examine the semi-crystalline nature of the PCL related materials. The samples were scanned from 5° to 50°, and only 20° to 25° were plotted because no prominent peaks were observed in the rest scattering angles, and fine details within 20° to 25° can be clearly viewed. The intensity versus diffraction angles for all three samples are plotted in Figure 11 and the analysis is shown in Table II. For all three samples, two sharp and distinct peaks can be seen around 21.4° and 23.7°, which are the representative peaks for PCL and indicates that the samples are highly crystalline materials.^{78–80} The peak intensity for the cPCL foam is decreased compared to the PCL reagent, which is due to crosslinking and 40% by volume of glass spheres. For the 280% tension programmed cPCL foam, the peak area of the amorphous domains is decreased significantly. The crystallinity is calculated based on (% crystallinity) = (the two peak areas of the crystalline domain) / (the two peak areas of the crystalline domain + the peak area of the amorphous domain). The programmed cPCL foam has smaller amorphous content which leads to a higher crystallinity. The full width at half maximum (FWHM) is inversely proportional to the crystal domain size (Scherrer Equation). Comparing the values of the PCL reagent and cPCL foam in Table II, the PCL reagent has larger crystal domain. This is because crosslinking influenced the polymer chain alignment and mobility, and lowered the packing ability so that the melting point, crystallinity, and domain size are all decreased.

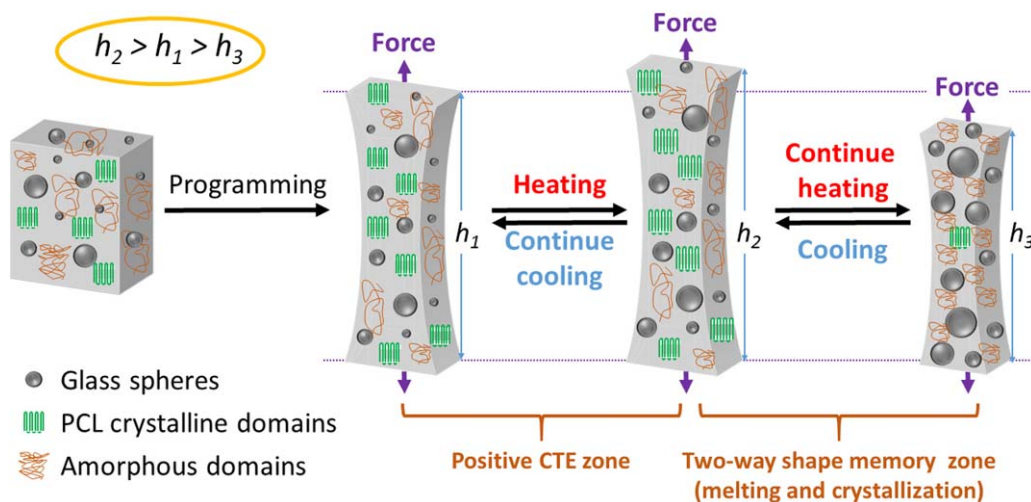


Figure 12. Proposed mechanism for the 2W-SME of the cPCL syntactic foam. [Color figure can be viewed at wileyonlinelibrary.com]

However, after 280% tension programming for the cPCL foam, there is a decrease in FWHM value which indicates an increase in the crystallinity.

Mechanism Elucidation

Based on the experimental results, the proposed mechanism for the 2W-SME of the cPCL foam is presented in Figure 12. For the as-prepared cPCL foam, there exist the crystalline domains for the PCL (as evidenced by the XRD result with 44.8% crystallinity in Table II), the amorphous PCL domains and the glass spheres with varying sizes. With a tension programming step (heating the foam, stretching the foam to a certain strain, and cooling down to freeze the temporary shape), there was an increase in the crystallinity (crystal size and amount), which was commonly defined as strain-induced crystallization (SIC). There was no influence on the glass spheres by the programming step. The transitions of the cPCL foam after programming were divided into two zones, a positive CTE zone where material elongates upon heating and contracts upon cooling, and a two-way shape memory zone where material elongates upon cooling and contracts upon heating. Continuously heating above the two-way shape memory zone will lead to melting of the crystallites and the material will be softened. With the temperature in the positive CTE zone, both the cPCL matrix and glass spheres behaved following the common physics, i.e., expansion upon heating and contraction upon cooling. However, within the melting and crystallization transition zone, the cPCL matrix behaved differently from the glass spheres. The crystalline domains melted during heating which induced contraction of the foam while the glass spheres still expanding. However, the expansion level of the glass spheres is much smaller than the contraction of the cPCL matrix, leading to contraction upon heating for the foam. During cooling, the formation of the crystalline domains under the constant external load induced obvious elongation of the cPCL matrix. Even though the volume of the cPCL decreased under the load due to the contraction of the unit cell perpendicular to the stretching direction, the growth of the unit cell parallel to the stretching direction leads to the obvious elongation of the cPCL.⁸¹ Similarly, this unusual expansion upon cooling for the cPCL matrix exceeds the usual contraction upon cooling for the glass microspheres, leading to expansion upon cooling for the foam. After a one-time tension programming, this unique two-way shape memory effect can continuously happen with a proper selection of external load and temperature range (Figure 5). Furthermore, by intentionally selecting the temperature range, the foam can perform only in the positive CTE zone, or the two-way shape memory zone, or both zones repeatedly after the one-time tension programming.

CONCLUSIONS

A two-way shape memory syntactic foam was successfully prepared with crosslinked polycaprolactone (cPCL) and glass microspheres. The bidirectional reversible actuation was around 10% strain with a relatively large initial programming strain, i.e., 134%. Programming was shown to be the key parameter to tune a prominent 2W-SME of the cPCL syntactic foam. However, at non-programmed state, the cPCL foam still displayed a

slight 2W-SME as demonstrated in the CTE study because the semicrystalline nature of the material (44.8% crystallinity based on XRD). The melting point of the cPCL foam was 47 °C based on DSC and the glass transition temperature was -24 °C from the tan delta curve acquired from DMA. This cPCL foam also possessed great one-way shape memory effect with >99% shape fixity ratio and >98% shape recovery ratio after the first shape memory cycle. The recovery stress of 80% compression programmed cPCL foam at 50 °C was 0.19 MPa. The heating induced contraction and cooling induced expansion are asymmetry, due to the incorporation of 40% by volume of glass microspheres, which has regular thermal behavior.

ACKNOWLEDGMENTS

The authors gratefully acknowledge the financial support by National Science Foundation under grant number CMMI 1333997, NASA cooperative agreement NNX16AQ93A under contract number NASA/LEQSF(2016-19)-Phase3-10, and Army Research Office under grant number W911NF-13-1-0145.

REFERENCES

1. Lee, S. T.; Park, C. B.; Ramesh, N. S. *Polymer Foams: Science and Technology*; CRC Press: Boca Raton, FL, 2006.
2. Jacobs, L. J. M.; Kemmere, M. F.; Keurentjes, J. T. F. *Green Chem.* 2008, 10, 731.
3. Hedrick, J.; Labadie, J.; Russell, T.; Hofer, D.; Wakharker, V. *Polymer* 1993, 34, 4717.
4. Sauceau, M.; Fages, J.; Common, A.; Nikitine, C.; Rodier, E. *Prog. Polym. Sci.* 2011, 36, 749.
5. Arora, K. A.; Lesser, A. J.; McCarthy, T. J. *Macromolecules* 1998, 31, 4614.
6. Guo, A.; Javni, I.; Petrovic, Z. *J. Appl. Polym. Sci.* 2000, 77, 467.
7. Hale, R. C.; La Guardia, M. J.; Harvey, E.; Mainor, T. M. *Chemosphere* 2002, 46, 729.
8. Williams, J. M.; Wroblewski, D. A. *Langmuir* 1988, 4, 656.
9. Squeo, E. A.; Quadrini, F. *Smart Mater. Struct.* 2010, 19, 105002.
10. Gupta, N.; Nagorny, R. *J. Appl. Polym. Sci.* 2006, 102, 1254.
11. McElhanon, J. R.; Russick, E. M.; Wheeler, D. R.; Loy, D. A.; Aubert, J. H. *J. Appl. Polym. Sci.* 2002, 85, 1496.
12. Shogren, R. L.; Lawton, J. W.; Doane, W. M.; Tiefenbacher, K. F. *Polymer* 1998, 39, 6649.
13. Bhatnagar, S.; Hanna, M. A. *Trans. ASAE* 1995, 38, 567.
14. Lee, L. J.; Zeng, C. C.; Cao, X.; Han, X. M.; Shen, J.; Xu, G. *J. Compos. Sci. Technol.* 2005, 65, 2344.
15. Zeng, C. C.; Han, X. M.; Lee, L. J.; Koelling, K. W.; Tomasko, D. L. *Adv. Mater.* 2003, 15, 1743.
16. Chen, L. M.; Rende, D.; Schadler, L. S.; Ozisik, R. *J. Mater. Chem. A* 2013, 1, 3837.
17. Xu, Q.; Ren, X. W.; Chang, Y. N.; Wang, J. W.; Yu, L.; Dean, K. *J. Appl. Polym. Sci.* 2004, 94, 593.
18. Filova, E.; Jakubcova, B.; Danilova, I.; Kostakova, E. K.; Jarosikova, T.; Chernyavskiy, O.; Hejda, J.; Handl, M.;

- Beznoska, J.; Necas, A.; Rosina, J.; Amler, E. *Physiol. Res.* **2016**, *65*, 121.
19. Jenkins, M. J.; Harrison, K. L.; Silva, M.; Whitaker, M. J.; Shakesheff, K. M.; Howdle, S. M. *Eur. Polym. J.* **2006**, *42*, 3145.
20. Di Maio, E.; Mensitieri, G.; Iannace, S.; Nicolais, L.; Li, W.; Flumerfelt, R. W. *Polym. Eng. Sci.* **2005**, *45*, 432.
21. Salerno, A.; Di Maio, E.; Iannace, S.; Netti, P. A. *J. Porous Mater.* **2012**, *19*, 181.
22. Salerno, A.; Iannace, S.; Netti, P. A. *Macromol. Biosci.* **2008**, *8*, 655.
23. Salerno, A.; Di Maio, E.; Iannace, S.; Netti, P. A. *J. Supercrit. Fluids* **2011**, *58*, 158.
24. Tsimpliaraki, A.; Tsivintzelis, I.; Marras, S. I.; Zuburtikudis, I.; Panayiotou, C. *J. Supercrit. Fluids* **2013**, *81*, 86.
25. Lu, L.; Li, G. *ACS Appl. Mater. Interfaces* **2016**, *8*, 14812.
26. Thomsen, D. L.; Keller, P.; Naciri, J.; Pink, R.; Jeon, H.; Shenoy, D.; Ratna, B. R. *Macromolecules* **2001**, *34*, 5868.
27. Dolynchuk, O.; Kolesov, I.; Radusch, H.-J. *Polym Adv. Technol.* **2014**, *25*, 1307.
28. Ma, L.; Zhao, J.; Wang, X.; Chen, M.; Liang, Y.; Wang, Z.; Yu, Z.; Hedden, R. C. *Polymer* **2015**, *56*, 490.
29. Seok Jin, H.; Woong-Ryeol, Y.; Ji Ho, Y. *Smart Mater. Struct.* **2010**, *19*, 035022.
30. Chen, S.; Hu, J.; Zhuo, H.; Zhu, Y. *Mater. Lett.* **2008**, *62*, 4088.
31. Chen, S.; Hu, J.; Zhuo, H. *Compos. Sci. Technol.* **2010**, *70*, 1437.
32. Raquez, J.-M.; Vanderstappen, S.; Meyer, F.; Verge, P.; Alexandre, M.; Thomassin, J.-M.; Jérôme, C.; Dubois, P. *Chem.—Eur. J.* **2011**, *17*, 10135.
33. Bothe, M.; Pretsch, T. *Macromol. Chem. Phys.* **2012**, *213*, 2378.
34. Behl, M.; Kratz, K.; Zotzmann, J.; Nöchel, U.; Lendlein, A. *Adv. Mater.* **2013**, *25*, 4466.
35. Qin, H.; Mather, P. T. *Macromolecules* **2009**, *42*, 273.
36. Basit, A.; Hostis, G.; Pac, M.; Durand, B. *Materials* **2013**, *6*, 4031.
37. Wang, Z.; Song, W.; Ke, L.; Wang, Y. *Mater. Lett.* **2012**, *89*, 216.
38. Xie, T.; Li, J.; Zhao, Q. *Macromolecules* **2014**, *47*, 1085.
39. Qi, G.; Kristofer, K. W.; Patrick, T. M.; Martin, L. D.; Qi, H. *J. Smart Mater. Struct.* **2013**, *22*, 055009.
40. Chung, T.; Romo-Uribe, A.; Mather, P. T. *Macromolecules* **2008**, *41*, 184.
41. Westbrook, K. K.; Parakh, V.; Chung, T.; Mather, P. T.; Wan, L. C.; Dunn, M. L.; Qi, H. *J. Eng. Mater. Technol.* **2010**, *132*, 041010.
42. Li, J.; Rodgers, W. R.; Xie, T. *Polymer* **2011**, *52*, 5320.
43. Behl, M.; Kratz, K.; Noechel, U.; Sauter, T.; Lendlein, A. *Proc. Natl. Acad. Sci. U.S.A.* **2013**, *110*, 12555.
44. Razzaq, M. Y.; Behl, M.; Kratz, K.; Lendlein, A. *Adv. Mater.* **2013**, *25*, 5730.
45. Razzaq, M. Y.; Behl, M.; Nöchel, U.; Lendlein, A. *Polymer* **2014**, *55*, 5953.
46. Tippets, C. A.; Li, Q.; Fu, Y.; Donev, E. U.; Zhou, J.; Turner, S. A.; Jackson, A.-M. S.; Ashby, V. S.; Sheiko, S. S.; Lopez, R. *ACS Appl. Mater. Interfaces* **2015**, *7*, 14288.
47. Zhou, J.; Turner, S. A.; Brosnan, S. M.; Li, Q.; Carrillo, J.-M. Y.; Nykypanchuk, D.; Gang, O.; Ashby, V. S.; Dobrynin, A. V.; Sheiko, S. S. *Macromolecules* **2014**, *47*, 1768.
48. Turner, S. A.; Zhou, J.; Sheiko, S. S.; Ashby, V. S. *ACS Appl. Mater. Interfaces* **2014**, *6*, 8017.
49. Haberl, J. M.; Sánchez-Ferrer, A.; Mihut, A. M.; Dietsch, H.; Hirt, A. M.; Mezzenga, R. *Adv. Funct. Mater.* **2014**, *24*, 3179.
50. Huang, M.; Dong, X.; Wang, L.; Zhao, J.; Liu, G.; Wang, D. *RSC Adv.* **2014**, *4*, 55483.
51. Pandini, S.; Passera, S.; Messori, M.; Paderni, K.; Toselli, M.; Gianoncelli, A.; Bontempi, E.; Riccò, T. *Polymer* **2012**, *53*, 1915.
52. Pandini, S.; Dioni, D.; Paderni, K.; Messori, M.; Toselli, M.; Bontempi, E.; Riccò, T. *J. Intell. Mater. Syst. Struct.* **2016**, *27*, 1388.
53. Meng, Y.; Jiang, J.; Anthamatten, M. *ACS Macro Lett.* **2015**, *4*, 115.
54. Zotzmann, J.; Behl, M.; Hofmann, D.; Lendlein, A. *Adv. Mater.* **2010**, *22*, 3424.
55. Saatchi, M.; Behl, M.; Nöchel, U.; Lendlein, A. *Macromol. Rapid Commun.* **2015**, *36*, 880.
56. Stroganov, V.; Al-Hussein, M.; Sommer, J.-U.; Janke, A.; Zakharchenko, S.; Ionov, L. *Nano Lett.* **2015**, *15*, 1786.
57. Lee, K. M.; Knight, P. T.; Chung, T.; Mather, P. T. *Macromolecules* **2008**, *41*, 4730.
58. Bai, Y.; Zhang, X.; Wang, Q.; Wang, T. *J. Mater. Chem. A* **2014**, *2*, 4771.
59. Baker, R. M.; Henderson, J. H.; Mather, P. T. *J. Mater. Chem. B* **2013**, *1*, 4916.
60. Li, G. *Self-Healing Composites: Shape Memory Polymer Based Structures*; Wiley: West Sussex, UK, **2014**.
61. Li, G.; Jones, N. *Compos. Part A* **2007**, *38*, 1483.
62. Li, G.; Xu, T. *J. Transport. Eng. ASCE* **2011**, *137*, 805.
63. Lawrence, E.; Pyrz, R. *Polym. Polym. Compos.* **2001**, *9*, 227.
64. Mae, H.; Omiya, M.; Kishimoto, K. *Mater. Sci. Eng. A* **2008**, *477*, 168.
65. John, M.; Li, G. *Smart Mater. Struct.* **2010**, *19*, 075013.
66. Li, G.; Uppu, N. *Compos. Sci. Technol.* **2010**, *70*, 1419.
67. Li, G.; Nettles, D. *Polymer* **2010**, *51*, 755.
68. Xu, W.; Li, G. *Int. J. Solids Struct.* **2010**, *47*, 1306.
69. Gupta, N.; Zeltmann, S. E.; Shunmugasamy, V. C.; Pinisetty, D. *JOM* **2014**, *66*, 245.
70. Coleman, M. M.; Zarian, J. *J. Polym. Sci. Part B: Polym. Phys.* **1979**, *17*, 837.
71. Elzein, T.; Nasser-Eddine, M.; Delaite, C.; Bistac, S.; Dumas, P. *J. Colloid Interface Sci.* **2004**, *273*, 381.
72. Bibin, J.; Reghunadhan Nair, C. P. Update on Syntactic Foams; ChemTec Publishing, iSmithers, UK, **2010**.

73. Gök, M. O.; Bilir, M. Z.; Gürcüm, B. H. *Procedia Soc. Behav. Sci.* **2015**, *195*, 2160.
74. Zhang, F. H.; Zhou, T. Y.; Liu, Y. J.; Leng, J. S. *Sci. Rep.* **2015**, *5*, 1.
75. Lendlein, A.; Kelch, S. *Angew. Chem. Int. Ed.* **2002**, *41*, 2034.
76. Li, G.; Xu, W. *J. Mech. Phys. Solids* **2011**, *59*, 1231.
77. Xu, W.; Li, G. *J. Appl. Mech.* **2011**, *78*, 061017.
78. Sravanthi, R. Master Thesis, National Institute of Technology, **2009**.
79. Wu, C.-S. *J. Appl. Polym. Sci.* **2004**, *94*, 1000.
80. Ha, J. C.; Kim, S. Y.; Lee, Y. M. *J. Control. Release* **1999**, *62*, 381.
81. Tosaka, M.; Murakami, S.; Poompradub, S.; Kohjiya, S.; Ikeda, Y.; Toki, S.; Sics, I.; Hsiao, B. S. *Macromolecules* **2004**, *37*, 3299.